Published in final edited form as:
Neuroscience. 2010 December 15; 171(3): 637–654. doi:10.1016/j.neuroscience.2010.09.055.

Postnatal development of NMDA receptor subunits 2A, 2B, 2C, 2D, and 3B immunoreactivity in brain stem respiratory nuclei of the rat

QIULI LIU[1] and **MARGARET T.T. WONG-RILEY**[1]

[1]Department of Cell Biology, Neurobiology and Anatomy, Medical College of Wisconsin, Milwaukee, Wisconsin, 53226, USA

Abstract

Previously, we reported that a critical period in respiratory network development exists in rats around postnatal days P12-13, when abrupt neurochemical, metabolic, and physiological changes occur. Specifically, the expressions of glutamate and NMDA receptor (NR) subunit 1 in the pre-Bötzinger complex (PBC), nucleus ambiguus (Amb), hypoglossal nucleus (XII), and ventrolateral subnucleus of solitary tract nucleus (NTS_{VL}) were significantly reduced at P12. To test our hypothesis that other NR subunits also undergo postnatal changes, we undertook an in-depth immunohistochemical study of NR2A, 2B, 2C, 2D, and 3B in these four respiratory nuclei in P2-P21 rats, using the non-respiratory cuneate nucleus (CN) as a control. Our results revealed that: 1) NR2A expression increased gradually from P2 to P11, but fell significantly at P12 in all four respiratory nuclei (but not in the CN), followed by a quick rise and a relative plateau until P21; 2) NR2B expression remained relatively constant from P2 to P21 in all five nuclei examined; 3) NR2C expression had an initial rise from P2 to P3, but remained relatively constant thereafter until P21, except for a significant fall at P12 in the PBC; 4) NR2D expression fell significantly from P2 to P3, then plateaued until P12, and declined again until P21; and 5) in contrast to NR2D, NR3B expression rose gradually from P2 to P21. These patterns reflect a dynamic remodeling of NMDA receptor subunit composition during postnatal development, with a distinct reduction of NR2A expression during the critical period (P12), just as NR1 did in various respiratory nuclei. There was also a potential switch between the neonatal NR2D and the more mature NR3B subunit, possibly around the critical period. Thus, during the critical period, NMDA receptors are undergoing greater adjustments that may contribute to attenuated excitatory synaptic transmission in the respiratory network.

Keywords

critical period; glutamate receptors; hypoglossal nucleus; nucleus ambiguus; nucleus tractus solitarius; Pre-Bötzinger complex

Corresponding Author: Margaret T.T. Wong-Riley, Ph.D., Department of Cell Biology, Neurobiology, and Anatomy, Medical College of Wisconsin, 8701 Watertown Plank Road, Milwaukee, WI 53226, Tel.: 1 414 456 8467, Fax: 1 414 456 6517 mwr@mcw.edu.

A critical period of postnatal development in the respiratory network of rats was characterized in our previously studies (Liu and Wong-Riley, 2002; Liu et al., 2003; Liu and Wong-Riley, 2003; Liu and Wong-Riley, 2005; Wong-Riley and Liu, 2005; Liu et al., 2006; Wong-Riley and Liu, 2008; Liu et al., 2009). This is a narrow window at the end of the second postnatal (P) week (around P12-13), when abrupt neurochemical, metabolic, and physiological changes occur in the brain stem respiratory network. During this time, there is a transient imbalance between the expressions of excitatory and inhibitory neurochemicals, such that the levels of inhibitory neurotransmitters (GABA) and receptors ($GABA_B$ and glycine receptors) are significantly increased, whereas those of the excitatory ones (glutamate and *N*-methyl-D-aspartate or NMDA receptor subunit 1) precipitously fall. At the same time, there is a sudden decrease in the activity of a metabolic marker of neuronal activity, cytochrome oxidase, in various respiratory nuclei (Liu and Wong-Riley, 2002; Liu et al., 2003; Liu and Wong-Riley, 2003; Liu and Wong-Riley, 2005; Wong-riley and Liu, 2005; 2008), and the animals' ventilatory and metabolic responses to hypoxia are also at their weakest (Liu et al., 2006; 2009).

To explore additional mechanisms that may underlie the critical period, we analyzed subunit expressions of $GABA_A$ receptors that mediate the majority of fast inhibitory synaptic interactions in the adult mammalian brain. We found that the developmental trend of α3 subunit decreases with age, whereas that of α1 increases with age, and the two intersect at P12 (Liu and Wong-Riley, 2004; 2006). Subunit switches may underlie a change in $GABA_A$ receptor subtype that may mediate a transition from a less efficient inhibitory transmission before P12 to a more mature one at P12 and thereafter, as suggested by a change in the kinetics of postsynaptic potentials during postnatal development in the thalamus and the visual cortex (Okada et al., 2000; Bosman et al., 2002).

Possible switches in subunit composition of the excitatory glutamatergic NMDA receptors have not been explored in brain stem respiratory nuclei. The present study aimed at testing our hypothesis that subunits of NMDA receptors (NR) undergo distinct changes during postnatal development, especially during the critical period in rats. An in-depth immunohistochemical study of NR2A, NR2B, NR2C, NR2D, and NR3B were conducted in P2 to P21 rats in the pre-Bötzinger complex (PBC, postulated as the center of respiratory rhythmogenesis; Smith et al., 1991; Rekling and Feldman, 1998; Smith et al., 2000), the nucleus ambiguus (Amb, which controls the upper airway muscles; Jordan, 2001), the hypoglossal nucleus (XII, which controls the tongue muscles associated with airway patency; Horner, 2007), and the ventrolateral subnucleus of the solitary tract nucleus [NTS_{VL}, which receives peripheral chemosensitive afferents (Finley and Katz, 1992) and is involved in respiratory modulation (Paton et al., 1991; Bonham, 1995)]. The non-respiratory cuneate nucleus (CN, a relay in the somatosensory system with no known respiratory function) was chosen as an internal control. Results were compared with those of NR1 analyzed previously (Liu and Wong-Riley, 2002; 2005).

Materials and Methods

Tissue preparation

All experiments and animal procedures were performed in accordance with the Guide for the Care and Use of Laboratory Animals (National Institutes of Health Publications No. 80-23, revised 1996), and all protocols were approved by the Medical College of Wisconsin Animal Care and Use Committee (approval can be provided upon request). All efforts were made to minimize the number of animals used and their suffering.

A total of 132 Sprague-Dawley rats, both male and female, from 11 litters were used. Rat pups were sacrificed at each of postnatal days P2 to P5, P7, P10-14, P17, and P21 (i.e., 12

time points, with 11 rats per time point for NR2A and 2B, and 5 rats per time point for the other NR subunits). Rats were deeply anesthetized with 4% chloral hydrate (1 ml/100 g IP; Fisher Scientific, Fair Lawn, NJ) and perfused through the aorta with 4% paraformaldehyde-4% sucrose in 0.1 M sodium phosphate buffered saline (PBS), pH 7.4. Brain stems were then removed and postfixed in the same fixative for 3 h at 4°C. They were subsequently cryoprotected by immersion in increasing concentrations of sucrose (10, 20, and 30%) in 0.1 M PBS at 4°C, then frozen on dry ice, and stored at −80°C until use.

Antibody characterization

Table 1 shows a brief summary of the antibodies used in the present study. All five antibodies (anti-NR2A, anti-NR2B, anti-NR2C, anti-NR2D, and anti-NR3B) have been well characterized and their specificities established by the manufacturers and previous investigators. The amino acid sequence of each of the synthetic peptides bore no sequence homology with any other peptides, and there was no cross-reactivity with any other known proteins. The anti-NR2A polyclonal antibody (AB1555P, Chemicon, Temecula, CA) was a purified immunoglobulin raised against a C-terminal fusion protein of rat NR2A (aa 1253-1391). By western blots it recognized a 180 kDa band in rat brain membranes, and did not react with NR2B or 2C. Immunolabeling was blocked by preadsorption of the antibody with the immunogen. The anti-NR2B polyclonal antibody (AB1557P, Chemicon) was a purified immunoglobulin raised against a C-terminal fusion protein of NR2B. It showed specific immunolabeling of the 180 kDa NR2B and no reactivity to NR2A or NR2C by western blots. The immunolabeling was blocked by preadsorption of the antibody with the C-terminal fusion protein used to generate the antibody. The anti-NR2C polyclonal antibody (sc-50437, Santa Cruz Biotech, Santa Cruz, CA) was raised against amino acids 21-100, mapping near the N-terminus of NR2C of human origin. By western blots it recognized a 135 kDa band. The anti-NR2D monoclonal antibody (MAB5578, clone 1G9.39A5, Chemicon) was raised against the C-terminal protein of rat NR2D and reacted with a band at ~145 kDa by western blots. The anti-NR3B polyclonal antibody (07-351, Upstate, Temecula, CA) was a purified immunoglobulin raised against amino acids 916-930 of mouse NR3B that recognized NR3B at ~98 kDa by western blots.

Immunohistochemistry

Coronal sections (12-μm thickness) of frozen brain stems were cut with a Leica CM1900 cryostat (Leica Microsystems, Heidelberger, Nussloch, Germany). Seven sets of serial sections were mounted on gelatin-coated slides. In the same litter, sections from 3 rats at different ages were mounted on the same slides so that they might be processed together. Ages were grouped typically as follows: P2-10-21, P3-4-17, P5-7-14, and P11-12-13. The first three sects showed the developmental trends, whereas the fourth set concentrated on the critical period. Having 3 distinct ages on the same slide ensured that any changes observed between ages were intrinsic to the animals and not as a result of unforeseen variations of tissue processing between slides. All sections from all rats were processed under identical conditions (i.e., time, temperature, and concentration of reagents). They were blocked overnight at 4°C with 5% nonfat dry milk-5% normal goat serum-1% Triton X-100 in 0.1 M PBS (pH 7.4). Sections were then incubated at 4°C for 36 h in the primary antibodies diluted at the proper concentration (Table 1) in the same solution as used for blocking. Sections were rinsed 3 times, 5 min each, in PBS, then incubated in the secondary antibodies: 1:100 goat anti-rabbit IgG-HRP (Bio-Rad, Hercules, CA) for NR2A, 2B, 2C, and 3B, and 1:100 goat anti-mouse IgG-HRP (Bio-Rad) for NR2D, diluted in the modified blocking solution (without Triton X-100) for 4 h at room temperature. After rinsing twice with PBS and once with 0.1 M ammonium phosphate buffer (APB), pH 7.0, immunoreactivity was detected with 0.05% DAB-0.004% H_2O_2 in APB for 5 min, and the reaction was stopped with APB for 5 min and then rinsed in PBS three times, dehydrated, and coverslipped. Control sections

were processed without primary antibodies or with a non-immune serum in place of the primary antibodies.

One set of alternate sections was reacted for neurokinin-1 receptors, using protocols described previously (Liu and Wong-Riley, 2002).

We used a non-respiratory nucleus, the cuneate nucleus (CN), as a negative control. CN is known for its relay function in somatosensory transduction but is not involved in respiratory functions.

Semi-quantitative optical densitometry

The immunoreactivity of different markers in the cytoplasm of neurons in various nuclei studied was semi-quantitatively analyzed by optical densitometric measurements of reaction product of immunohistochemistry, performed with a Zeiss Zonax MPM 03 photometer, a ×25 objective, and a 2-μm-diameter measuring spot. White (tungsten) light was used for illumination, and all lighting conditions were held constant for all of the measurements. Since light intensity can directly affect optical densitometric values, a stepped density filter (Edmund Industrial Optics, Barrington, NJ) with 10-step increments of 0.1 from 0.1 to 1, was used to precisely adjust the intensity of the light source to a standard value identical for all samples.

The boundary of each brain stem nucleus studied was determined with the aid of the Paxinos and Watson's "The Rat Brain Atlas" (Academic Press, New York, 1986). The PBC was identifiable with the neurokinin-1 receptor labeling (Gray et al., 1999), as described in our previous papers (Liu and Wong-Riley, 2002, 2003, 2005). The part of the nucleus ambiguus chosen for the present study (and our previous studies, Liu and Wong-Riley, 2003, 2005, 2008) was the semicompact formation and the rostral loose formation innervating upper airway muscles and representing pharyngolaryngomotor functions (Bieger and Hopkins, 1987). For the remaining nuclei, measurements were taken from the central main portion of each nucleus.

The optical densitometric value of each labeled neuron in the various brain stem nuclei studied was an average reading of two to four spots in the cytoplasm of its cell body (avoiding the portion that any immunoreactive process crossed the cell body). Only those neurons whose nuclei were clearly visible (i.e., sectioned through the middle of the cell body) were measured. To avoid measuring the same neuron more than once, values were taken from cells in sections at least 84 μm apart, as the largest neurons had a maximal diameter of 25–30 μm, with a maximal nuclear diameter of only about 10 μm. About 100 neurons in each brain stem nucleus were measured for each marker in each rat, and a total of about 1100 (for each of NR2A and 2B) or 500 neurons (for each of NR2C, 2D, and 3B) in each nucleus at each age were measured. For statistical analyses, each sample's optical density value for each nucleus of each rat was the average of about 100 labeled neurons. Thus, the sample number of each time point in each nucleus was eleven (for NR2A and 2B) or five (for NR2C, 2D, and 3B) (representing the number of animals) in Figures 2, 4, 6, 8, and 10. A total of 168,000 neurons were measured for the present study. Mean optical density values, standard deviations, and standard errors of the mean in each nucleus at each age were then obtained.

Statistical analysis

Statistical comparisons were made among the age groups by using one-way analysis of variance (ANOVA) (to control for the type I comparisonwise error rate) and, when significant differences were found, comparisons were made between one age group and its immediately younger age group (e.g., P2 vs. P3, P3 vs. P4, and P5 vs. P7) by using Tukey's

Studentized range test (a *post hoc* multiple comparisons, to control for the type I experimentwise error rate). Additional Tukey's tests were done between two groups of varying ages (not shown in graphs) within each nucleus for each NR subunit. Significance was set at $P < 0.01$ for one-way ANOVA and $P < 0.05$ for Tukey's test.

RESULTS

Statistical comparisons (ANOVA) of four time points: P2, P7, P12, and P21 for each receptor subunit (NR2A-2D and 3B) in each of the five brain stem nuclei revealed no significant differences in the percentage of labeled neurons among the ages tested. Figures 2, 4, 6, 8, and 10 show significance only between one age group and its immediately adjacent younger age group by means of the Tukey's test. Additional comparisons are described in the text below.

I. NR2A-immunoreactive (-ir) neurons in the brain stem nuclei

In general, NR2A-ir products were clearly visible in subpopulations of neurons in each of the brain stem nuclei examined (Fig. 1A-E). The size of NR2A-ir neurons increased with age and reached a relatively stable level after P11-P12 (Fig. 1A-E). Control sections demonstrated no specific immunoreactive product above background, and that was also true for controls of NR2B, NR2C, NR2D, and NR3B labeling (data not shown). ANOVA indicated significant differences ($P < 0.01$) in the intensity of NR2A-ir expression among the ages in all five nuclei examined, and Tukey's test indicated significant reductions at P12 as compared to P11 for all four respiratory nuclei tested ($P < 0.01$ for PBC and XII, and $P < 0.05$ for Amb and NTS_{VL}) but not for CN (Fig. 2). P12 was the only time point that yielded statistical significance when two adjacent ages were compared during the first three postnatal weeks.

A. NR2A-ir neurons in the PBC—NR2A immunoreactivity was observed in ~ 60% - 70% of neurons in the PBC. They were small or medium in size, and multipolar, granular, or fusiform in shape (Fig. 1A1-4). The size of small neurons ranged from 5.5 – 7 μm in diameter at P2 to 8.5 – 12.5 μm at P21, whereas medium-sized neurons ranged from 10 – 13 μm at P2 to 13.5 – 17.5 μm at P21. Immunoreactivity was observed in the cell bodies and proximal processes of neurons, but was at a low level in the rest of the neuropil (Fig. 1A1-4). The intensity of NR2A immunoreactivity in the somatic cytoplasm increased gradually with age from P2 to P11, then fell significantly at P12 ($P < 0.01$), followed by a slight increase at P13-14, and a gradual fall at P17 and P21 (Fig. 2A). With Tukey's test, there was a significant difference in labeling intensity between P3-4 and P11 ($P < 0.01$) and between P11 and P21 ($P < 0.01$), but not between P2 and P21.

B. NR2A-ir neurons in the Amb—About 65% - 80% of Amb neurons were NR2A-ir. Immunoreactivity was present in the cell bodies and proximal processes of neurons, but was low in the rest of the neuropil (Fig. 1B1-4). These neurons were multipolar or oval in shape, and mainly medium or small in size. The size of small neurons ranged from 8 – 9.5 μm in diameter at P2 to 9.5 – 13 μm at P21, whereas medium-sized neurons ranged from 11 – 14 μm at P2 to 14 – 17 μm at P21. The intensity of NR2A labeling showed a gradual rise from P2 to P11, then precipitously fell at P12 ($P < 0.05$), followed by a small rise at P13-14 and a further fall at P17 and P21 (Fig. 2B). Tukey's test also indicated a difference between P11 and P17 ($P < 0.05$) or P21 ($P < 0.001$).

C. NR2A-ir neurons in the XII—NR2A immunoreactivity was present in 65%- 75% of the XII neurons. These neurons were mainly medium or large in size and multipolar or pyramid-like in shape (Fig. 1C1-4). The size of medium neurons ranged from 12 – 15 μm in

diameter at P2 to 16 – 21 μm at P21, whereas large neurons ranged from 16 – 20 μm at P2 to 23 – 28 μm at P21. Immunoreactivity was present in the cell bodies and proximal processes of labeled neurons as well as in the neuropil (Fig. 1C1-4). The developmental trend of NR2A was very similar to that in the PBC, with a gradual rise from P2 to P11, a significant fall at P12 ($P < 0.01$), followed by a slight rise at P13-14, and a further but gentler decline at P17 and P21 (Fig. 2C). Comparisons of other, non-consecutive pairs of ages with Tukey's indicated a significant difference between P2 and P7 or P11 ($P < 0.01$ for both), between P11 and P14, P17, or P21 ($P < 0.01$ - $P < 0.001$), and between P3 and P21 ($P < 0.05$).

D. NR2A-ir neurons in the NTS_{VL}—NR2A-ir was visible in about 45% ~ 70% of the NTS_{VL} neurons that were small in size and mainly multipolar, oval, or granular in shape (Fig. 1D1-4). The size of small neurons ranged from 5 – 7.5 μm in diameter at P2 to 6.5 – 12 μm at P21. The developmental trend of NR2A expression in the NTS_{VL} neurons was comparable to those in the other three respiratory nuclei, with a gradual rise from P3 to P11, a significant decrease at P12 ($P < 0.05$), followed by a small rise and a gentle fall until P21 (Fig. 2D). Tukey's test also showed a significant difference between P3 or P4 and P11 ($P < 0.05$), and between P11 and P21 ($P < 0.05$).

E. NR2A-ir neurons in the CN—About 35% - 40% of the CN neurons exhibited NR2A-ir in their cell bodies (Fig. 1E1-4). Labeled neurons were mainly small in size and oval, multipolar, or granular in shape. The size of small neurons ranged from 5 – 8 μm in diameter at P2 to 7 – 11 μm at P21, whereas medium-sized neurons ranged from 9 – 11.5 μm at P2 to 12.5 – 15.5 μm at P21. The NR2A-ir expression in the CN neurons was relatively constant from P2 to P21, with some minor fluctuations (Fig. 2E). There were no significant day-to-day changes, only a difference between P4 and P10 ($P < 0.05$), indicating a development phase mainly during the first postnatal week.

II. NR2B-ir neurons in the brain stem nuclei

Generally, NR2B-ir products were clearly visible in subpopulations of neurons in all five brain stem nuclei examined (Fig. 3A-E). The sizes, developmental changes, shapes, and prevalence of labeled neurons were comparable to those of NR2A-ir neurons, and will not be described in detail below. ANOVA failed to reveal any significant difference ($P > 0.01$) in the NR2B-ir expression among the ages in all five nuclei examined.

A. NR2B-ir neurons in the PBC—About 60% - 70% of PBC neurons exhibited NR2B immunoreactivity that was distributed mainly in the cell bodies and some proximal processes (Fig. 3A1-4). The developmental expression of NR2B-ir in the PBC was relatively constant, with lower levels at P2-3 and P21, and the highest level at P11, but no significant difference between any two age groups (Fig. 4A).

B. NR2B-ir neurons in the Amb: About 65% - 80% of the Amb neurons demonstrated NR2B-ir in their cell bodies and some proximal processes (Fig. 3B1-4). The developmental trend was similar to that in the PBC, with fluctuations from P2 to P21 without any statistical significance among them (Fig. 4B).

C. NR2B-ir neurons in the XII: NR2B immunoreactivity was observed in the cell bodies and some proximal processes of ~ 70% - 90% of the XII neurons (Fig. 3C1-4). The developmental expression of NR2B-ir in the XII was also relatively constant with some fluctuations from P2 to P21, with higher expression at P5 and P7 than at P21 ($P < 0.05$ for both) (Fig. 4C).

D. NR2B-ir neurons in the NTS_{VL}: There were ~ 35% - 50% of the NTS_{VL} neurons that exhibited NR2B-ir in their cell bodies and some proximal processes (Fig. 3D1-4). The expression was relatively constant throughout the first three postnatal weeks, with slightly lower values in the first week and higher values thereafter until P21 (Fig. 4D). There was no significant difference between any two age groups.

E. NR2B-ir neurons in the CN: NR2B immunoreactivity was present in about 50% - 80% of the CN neurons and was mainly in their cell bodies and some proximal processes (Fig. 3E1-4). The expression was relatively constant, with lower levels at P2-4 and P21, and higher level at P11-12, but no significant difference between any two age groups (Fig. 4E).

III. NR2C-ir neurons in the brain stem nuclei—NR2C immunoreactivity was clearly observed in subpopulations of neurons in each of the brain stem nuclei examined (Fig. 5A-E). Labeling was present in the cell bodies and proximal processes of neurons and in the rest of the neuropil. The size of labeled neurons increased with age and reached a relatively stable level after P10-P11. The shapes and sizes of immunoreactive neurons were similar to those with NR2A-ir, and will not be described in detail below. Generally, the developmental trends of NR2C-ir in the five nuclei examined were similar, with the lowest level at P2, an increase (with or without statistical significance) at P3, followed by a plateau thereafter. A clear exception was the PBC, where a significant reduction in NR2C-ir occurred at P12 ($P < 0.05$). ANOVA revealed significant differences ($P < 0.01$) in the NR2C-ir expression among the ages in the PBC and XII, and Tukey's test indicated a significant reduction at P12 for the PBC and a significant rise at P3 for the PBC and XII (Fig. 6A and 6C).

A. NR2C-ir neurons in the PBC: About 60% - 80% of the PBC neurons demonstrated NR2C-ir in their cell bodies and some proximal processes (Fig. 5A1-4). Generally, the expression of NR2C-ir in the PBC neurons increased with age, with a significant rise at P3 ($P < 0.05$) and a significant difference between P2 or P3 and P11 ($P < 0.01$-0.001). However, there was also a significant fall at P12 ($P < 0.05$) (Fig. 6A). In addition, the increase in labeling from P2 to P21 was significant ($P < 0.01$).

B. NR2C-ir neurons in the Amb: NR2C immunoreactivity was present in about 70% - 80% of the Amb neurons and was distributed mainly in their cell bodies and some proximal processes (Fig. 5B1-4). The expression was the lowest at P2, with a statistically insignificant rise at P3, followed by a plateau until P21 (Fig. 6B).

C. NR2C-ir neurons in the XII: Approximately 70% - 85% of the XII neurons exhibited NR2C immunoreactivity in their cell bodies and some proximal processes (Fig. 5C1-4). The expression was the lowest at P2, with a significant rise at P3 ($P < 0.05$), followed by a plateau until P21 (Fig. 6C).

D. NR2C-ir neurons in the NTS_{VL}: NR2C-ir was observed in about 50% - 60% of the NTS_{VL} neurons (Fig. 5D1-4). The expression gradually increased from P2 to P10, then exhibited a statistically insignificant reduction at P11-P12, followed by a plateau thereafter until P21 (Fig. 6D). There were no significant differences between any two age groups.

E. NR2C-ir neurons in the CN: NR2C-ir was observed in about 60% - 75% of the CN neurons (Fig. 5E1-4). The expression was lowest at P2, but remained relatively constant from P2 to P21 (Fig. 6E). The only significant difference among all the age groups was between P2 and P13 ($P < 0.05$).

IV. NR2D-ir neurons in the brain stem nuclei—Immunoreactivity for NR2D was clearly observed in subpopulations of neurons in each of the brain stem nuclei examined. It was distributed mainly in the cell bodies and some proximal processes, as well as in the neuropil (Fig. 7A-E). The sizes and shapes of NR2D-ir neurons were similar to those with NR2A-ir, and will not be described in detail below. The expression of NR2D in all five nuclei examined shared similar developmental trends, with the highest level at P2, declining significantly at P3 (not significant for CN), followed by a plateau until P12, at which a further decrease ensued through P17-21 (Fig. 8A-E). ANOVA yielded significant differences ($P < 0.01$) among the ages in each of the nuclei examined, and Tukey's test indicated a significant reduction at P3 for the PBC, Amb, XII, NTS_{VL}, and another significant reduction at P17 for the XII and CN (Fig. 8A-E).

A. NR2D-ir neurons in the PBC: NR2D-ir was observed in about 50% - 60% of the PBC neurons and was distributed mainly in their cell bodies and some proximal processes (Fig. 7A1-4). The expression decreased progressively with age, with a significant reduction at P3 ($P < 0.05$) and a statistically insignificant rise at P12 (Fig. 8A). Additional Tukey's test revealed significant differences between P2 and P11, between P2 or P3 and P21, and between P12 and P21 ($P < 0.001$ for all).

B. NR2D-ir neurons in the Amb: About 65% - 85% of the Amb neurons demonstrated NR2D-ir in their cell bodies and some proximal processes (Fig. 7B1-4). The developmental trend of immunoreactivity was comparable to that in the PBC, including a general decline with age, a significant reduction at P3 ($P < 0.05$), and a statistically insignificant rise at P12 (Fig. 8B). Additional Tukey's comparisons showed significant differences between the same age groups as described above for the PBC.

C. NR2D-ir neurons in the XII: NR2D immunoreactivity was observed in about 60% - 75% of the XII neurons and was distributed in their cell bodies and some proximal processes (Fig. 7C1-4). The expression was significantly decreased at P3 and P17 ($P < 0.01$ for both), but a rise at P12 was statistically insignificant (Fig. 8C). The age-dependent decline in labeling intensity was verified by further Tukey's test, which showed significant differences between the same age groups as described above for the PBC. In addition, there was also a significant difference between P12 and P17 ($P < 0.01$).

D. NR2D-ir neurons in the NTS_{VL}: NR2D-ir was exhibited in ~ 40% - 55% of the NTS_{VL} neurons (Fig 7D1-4). The expression was significantly reduced at P3 ($P < 0.001$), followed by a gradual decline until P21, except for statistically insignificant rises at P10-P11 and P13 (Fig. 8D). There were statistically significant differences between P2 or P3 and P21 ($P <$ 0.01-0.001), as well as between P2 and P7 ($P < 0.001$) and between P10 and P21 ($P < 0.01$).

E. NR2D-ir neurons in the CN: About 40% - 65% of the CN neurons demonstrated NR2D immunoreactivity (Fig. 7E1-4). The trend was a general decline with age, especially between P2 and P4 and between P12 and P17, with a statistically insignificant rise at P12. The fall from P14 to P17 was significant ($P < 0.05$) (Fig. 8E). Additional Tukey's comparisons revealed significant differences between the same age groups as described above for the XII.

IV. NR3B-ir neurons in the brain stem nuclei—NR3B-ir was present in subpopulations of neurons in each of the brain stem nuclei examined. It was distributed mainly in their cell bodies and some proximal processes, as well as in the rest of the neuropil (Fig. 9A-E). The sizes and shapes of NR2D-ir neurons shared common features as described above, and will not be elaborated below. Generally, the intensity of NR3B-ir expression in

the PBC, Amb, XII, and NTS_{VL} increased with age, with a statistically insignificant reduction at P3 (except for NTS_{VL}) and P12, whereas that in the CN was relatively constant, with only minor fluctuations (Fig. 10A-D). ANOVA revealed significant differences ($P < 0.01$) among the ages in the PBC, Amb, XII, and NTS_{VL}, indicating a general rise with age, but Tukey's test failed to yield a statistical significance in any comparison between pairs of adjacent age groups, indicating that the change was gradual (Fig. 10A-E). Additional Tukey's comparisons are described below.

A. NR3B-ir neurons in the PBC: NR3B immunoreactivity was observed in about 60% - 80% of the PBC neurons (Fig. 9A1-4). The distribution was mainly in the cell bodies and some proximal processes. There was a statistically insignificant dip at P3 followed by a gradual increase until P21 (Fig. 10A). Additional Tukey's test revealed a significant difference between P2 and P21 ($P < 0.05$) and between P3 and P21 ($P < 0.001$).

B. NR3B-ir neurons in the Amb: About 70% - 85% of the Amb neurons exhibited NR3B-ir in their cell bodies and proximal processes (Fig. 9B1-4). The developmental trend of immunoreactivity was similar to that in the PBC, with a statistically insignificant reduction at P3 followed by gradual increase until P21 (Fig. 10B). Additional Tukey's analysis showed the same level of significant differences between P2 or P3 and P21 as those in the PBC.

C. NR3B-ir neurons in the XII: NR3B-ir was present in 75% - 85% of the XII neurons (Fig. 9C1-4). The developmental trend was a general increase with age, but with a striking but statistically insignificant fall at P12 (Fig. 10C). Additional Tukey's analysis showed the same level of significant differences between P2 or P3 and P21 as those in the PBC. Moreover, there was also a significant difference between P3 and P10 ($P < 0.001$).

D. NR3B-ir neurons in the NTS_{VL}: NR3B-ir was observed in ~ 40% - 60% of the NTS_{VL} neurons (Fig. 9D1-4). The expression exhibited the lowest value at P2, a gradual increase until P10, followed by a plateau thereafter until P21 (Fig. 10D). The main statistically significant differences were between P2 and P4 ($P < 0.05$) and between P2 and P10 ($P < 0.01$).

E. NR3B-ir neurons in the CN: Approximately 55% - 70% of the CN neurons exhibited NR3B immunoreactivity (Fig. 9E1-4). The expression was relatively stable from P2 to P21, with a gentle rise and some fluctuations with age (Fig. 10E). The main statistically significant differences were between P2 and P10 ($P < 0.05$) and between P2 and P14 ($P < 0.05$).

DISCUSSION

The present study represents the first time that five different NMDA receptor subunits are analyzed in depth in five different brain stem nuclei during the first three postnatal weeks in rats. Our comprehensive analysis revealed that: 1) NR2A expression in all four respiratory nuclei and NR2C expression in the PBC were significantly reduced at P12, similar to a reduction at P12 for NR1 reported previously (Liu and Wong-Riley, 2002; 2005), but not in the non-respiratory CN. 2) The expression of NR2C was significantly increased at P3 in the PBC and XII (and rising though not reaching significance at P3 in the Amb and NTS_{VL}), whereas that of NR2D was significantly reduced at P3 in the PBC, Amb, XII, and NTS_{VL}. No comparable changes were observed in the CN. 3) The expression of NR2D generally decreased with age, whereas that of NR3B generally increased with age; and 4) the expression of NR2B stayed relatively constant throughout the first three postnatal weeks in rats.

General functions of NMDA receptors—Functional NMDA receptors are generally heterotetramers consisting of two obligatory NR1 subunits and two regulatory subunits composed of various combinations of four types of NR2 subunits (NR2A, NR2B, NR2C, and NR2D) and two types of NR3 subunits (NR3A and NR3B) (Monyer et al., 1994, Yashiro and Philpot, 2008). Functional properties of the NMDA channels depend on the precise combination of NMDA receptor subunits (Cull-Candy and Leszkiewicz, 2004). The NR1 subunit has eight functional isoforms arising from a single gene but varying in combinations of three independent splice variants, being critical in determining certain key features (Prybylowski et al., 2001; Cull-Candy and Leszkiewicz, 2004). The various NR2 subunits are essential for determining many biophysical and pharmacological properties of the NMDA receptors (Cull-Candy and Leszkiewicz, 2004). For channel opening property, NR1/NR2A di-heteromers possess faster rise and shorter decay time than the NR1/NR2B and NR1/NR2C channels, whereas NR2D-containing NMDARs have the slowest decay times (Chen et al., 1999; Cull-Candy and Leszkiewicz, 2004; Erreger et al., 2005). A typical or “conventional” NMDA receptor consists of two glycine-binding NR1 subunits and two glutamate-binding NR2 subunits to form a tetrameric channel that is highly permeable to Ca^{2+} and sensitive to voltage-dependent inhibition by Mg^{2+} (Chatterton et al., 2002; Cavara et al., 2009). However, NR3A or NR3B co-assemble with NR1 to form excitatory glycine receptors that are unaffected by glutamate or NMDA, are relatively Ca^{2+} impermeable, and are resistant to Mg^{2+}, MK-801, and other competitive antagonists (Chatterton et al., 2002; Cavara et al., 2009). When coexpressed with NR1 and NR2A in heterologous cells, NR3B reduced calcium permeability of glutamate-induced current, acting as a dominant modulatory subunit that can modify the function of NMDA receptors (Nishi, et al., 2001; Matsuda, et al., 2002). NR3A (not analyzed in the present study) share properties comparable to those of NR3B (Nishi, et al., 2001; Chatterton et al., 2002; Cavara et al., 2009). As substantiated in the present study, the expression of different NR2 subunits is both spatially and developmentally regulated, whereas that of NR1 subunit is sustained throughout (Watanabe et al., 1992; Monyer et al., 1994; Sheng et al., 1994; Kubota and Kitajima, 2008), albeit exhibiting some developmental changes as we reported previously (Liu and Wong-Riley, 2002; 2005).

NMDA receptors in the respiratory network—NMDA receptors are proposed to be essential and age-dependent for the generation and maintenance of respiratory rhythm under normoxic conditions (Feldman et al., 1992; Poon et al., 2000; Water and Machaalani, 2005; Morgado-Valle and Feldman, 2007; Pace et al., 2007). Their predominant effects in normal respiratory rhythmogenesis are the termination of inspiration (probably via a pontine synapse) and relay of peripheral chemorecptor inputs (via the solitary tract nucleus) (Pierrefiche et al., 1994; Dogaš et al., 1995; Water and Machaalani, 2005). NMDA receptors are also involved in response to exogenous stressors, such as hypoxia (Coles et al., 1998; Ohtake et al., 1998; 2000; Tarakanov et al., 2004; McGuire et al., 2005; Water and Machaalani, 2005; McGuire et al., 2008). The levels of NR2A/NR2B, in particular, are increased during intermittent hypoxia (Reeves et al., 2003), and they undergo greater tyrosine phosphorylation in dorsocaudal brain stem during hypoxia (Czapla et al., 1999). In the anoxic crucian carp brain, the expression of NR2B and NR2D predominates, comparable to that in the hypoxic-tolerant neonatal rats, and the expressions of NR1, NR2C, and NR3A were reduced (Ellefsen et al., 2008).

Each NR subunit immunoreactivity in each respiratory nucleus examined was present in the majority of neurons there (albeit of lower abundance in the CN for NR2A and 2D), implying that a sizeable population of neurons express a combination of NR2 and 3B subunits, in addition to the obligatory NR1. In different brain regions and various neuronal populations, there is evidence for the co-assembly of NR2A/NR2B, NR2A/NR2C, NR2B/NR2D, and others (Cull-Candy and Leszkiewicz, 2004). Such co-assembly is likely to increase the

variability of channel properties. Patch-clamp studies have demonstrated that the presence of these various assemblies have functional consequences and display distinct properties (Cathala et al., 2000; Brickley et al., 2003).

Functional implications—Our data point to a number of functional implications. First, the developmental trends of NR2A in the PBC, Amb, XII, and NTS_{VL} were comparable to those of NR1 in these same nuclei during the first two postnatal weeks as reported previously (Liu and Wong-Riley, 2002; 2005), all of which showed a significant reduction of subunit expression at P12. The sudden decrease in the expression of these subunits suggested an overall decrease in NR-mediated excitation during the critical period (see below). Second, a relatively constant level of NR2B expression during the first three postnatal weeks implies that this subunit is necessary for NR transmission, at least in the five nuclei examined. NR2B is known to play an important role in modifying synaptic plasticity during experience-dependent critical period and in long-term potentiation, as well as in learning and memory (Cull-Candy and Leszkiewicz, 2004; Barria and Malinow, 2005; Dumas, 2005; von Engelhardt et al., 2008). Third, NR2C was significantly increased at P3 and remained at a relative plateau thereafter. This subunit may also be essential to NR transmission in these nuclei. A significant reduction of NR2C expression in the PBC at P12 implies that it is down-regulated in concert with NR1 and NR2A during the critical period of respiratory network development. Fourth, there is strong evidence for a possible switch between the age-dependent decrease in NR2D and the age-dependent increase in NR3B, intersecting possibly around P13. Developmental changes between these two NR subunits may underlie important functional maturation in NR transmission in these four respiratory nuclei, with slower decay NR2D replaced by the faster decay NR3B, concomitant with respiratory functional maturation. Fifth, other than NR2D, all of the NR subunits tested showed a gradual increase in their expression from P2 to P11, before a significant or non-significant fall at P12. This indicates that NMDA receptors go through progressive maturation during the first 1 ½ postnatal weeks, but their expression was transiently suppressed during the critical period that may be associated with a decreased number of functional NMDA receptors. Finally, after the first two postnatal weeks and after the critical period, various combinations of NR2A, NR2B, NR2C, and NR3B appear to play a more important role than NR2D in teaming with NR1 for NMDA receptor-mediated synaptic transmission.

P0-P2—In neonatal rats, NR2D, with the highest level at P2 and decreasing with age thereafter, may play a more important role in NR transmission during prenatal and the first two days of postnatal life in the four respiratory nuclei examined, whereas NR2A, NR2C, and NR3B levels were low at that time (Monyer et al., 1994; Takahashi et al., 1996; Cathala et al., 2000; Matsuda et al., 2002; Liu et al., 2004; Durand et al., 2006; Kubota and Kitajima, 2008; and our present data). The immature, slower NR transmission (Cull-Candy and Leszkiewicz, 2004; Kron et al., 2008) coincides with the lowest cytochrome oxidase activity and glutamate level (Liu and Wong-Riley, 2002; 2003; 2005), and the slowest respiratory frequency and lowest tidal volume during normoxic ventilation at P0-P2 (Liu et al., 2006).

P3—At P3, a significant reduction in NR2D coincides with a significant increase in NR2C (with a decay time faster than that of NR2D but slower than that of NR2A) in the PBC, Amb, XII, and NTS_{VL}. The expressions of NR2A, NR2B, and NR3B were relatively low. This is also a time when cytochrome oxidase activity was decreased or at a plateau, and a transient imbalance between excitatory and inhibitory drives, with relatively low glutamate and NR1 levels (Liu and Wong-Riley, 2001; Liu and Wong-Riley, 2002; 2003; 2005). These events may be related to the animal's adaptation to postnatal gas conditions that occurs at about P2-4 in rats, especially in the NTS_{VL} that is important for peripheral chemosensitive

afferents (Finley and Katz, 1992). During the first two postnatal days, a sudden increase in arterial partial pressure of oxygen (Brouillette and Waxman, 1997) transiently suppresses peripheral chemosensitive organs (primarily the carotid bodies), which reset thereafter (Blanco et al., 1984; Mortola, 2001). We have shown previously that the ventilation and metabolic patterns of P0-1 rats were markedly different from those of P2 and older rats, both during normoxia and under hypoxia (Liu et al., 2009), with the lowest response to hypoxia at P3 among P0-P11 rats (Liu et al., 2006) and almost the lowest metabolic rate response to hypoxia at the same time (Liu et al., 2009).

Critical period (around P12)—Intriguingly, at P12 or the critical period, NR2A, 2C, 2D, and 3B expressions in the PBC, Amb, XII, and NTS_{VL} exhibited a change (with or without statistical significance) against their earlier development trends (except for NR2D in the NTS_{VL} in which its expression decreased, rather than increased). Specifically, a sudden, significant reduction in NR2A was evident in the PBC, Amb, XII, and NTS_{VL} and in NR2C in the PBC. The significant reduction in NR2A, with the fastest rise and shortest decay time (Chen et al., 1999; Cull-Candy and Leszkiewicz, 2004; Erreger et al., 2005), might markedly attenuate excitatory neurotransmission in all four respiratory nuclei. In the PBC and NTS_{VL}, it would result in reduced respiratory drive, especially under exogenous respiratory insults, such as hypoxia (Liu et al., 2006; 2009). In the Amb and XII, it would attenuate airway patency during respiration. The significant reduction of NR2C (with a decay time faster than that of NR2D) in the PBC may also contribute to reduced respiratory drive during critical period. These, together with a significant reduction in the expressions of glutamate and NR1 at P12 in the same nuclei (Liu and Wong-Riley, 2002; 2005), are likely to contribute to a transient attenuation in glutamatergic transmission via NRs within the respiratory network during the critical period. A brief increase in the expression of NR2D and a temporary decrease in that of NR3B at P12 may play a contributing but lesser role. Concomitantly, there was an increase in the expression of inhibitory neurochemicals (Liu and Wong-Riley, 2002; 2005), resulting in a transient imbalance between excitatory and inhibitory drives. During this critical period, ventilatory and metabolic rate responses to hypoxia were also significantly attenuated, making this a vulnerable period in respiratory development (Liu et al., 2006; 2009).

P13-14 and thereafter—At P13-14, a switch may occur between the neonatal NR2D and the more mature NR3B in several respiratory nuclei. This switch, together with higher expressions of NR2C and NR3B during the 3rd postnatal week, contribute to the maturation of the respiratory system, which includes an increases in tidal volume and a decrease in frequency with age, both during normoxia and under hypoxia (Liu et al., 2006). Notably, our presumed NR subunit switch occurs one or two day(s) later than that of $GABA_A$ α3 to α1 (at P12; Liu and Wong-Riley, 2004), indicating that the maturation of $GABA_A$ and NMDA receptors are not temporally in phase. The maturation of neurotransmission also coincides with a rise in cytochrome oxidase activity in the respiratory nuclei at P13 and thereafter, subsequent to a significant fall at P12 in multiple respiratory nuclei (Liu and Wong-Riley, 2002; 2003; Wong-Riley and Liu, 2005). Subunit switches and receptor maturation in both excitatory and inhibitory systems are important in the maturation of the entire respiratory network. In the mouse, the central respiratory network reportedly matures at P15 (Paton and Richter, 1995). In rats, the hypoxic and hypercapnic responses are found not to be mature until P15 or after (Eden and Hanson, 1987; Davis et al., 2006; Liu et al., 2006).

Acknowledgments

This study was supported by NIH grant HD048954.

Abbreviations

XII	hypoglossal nucleus
Amb	nucleus ambiguus
ANOVA	analysis of variance
APB	ammonium phosphate buffer
CN	cuneate nucleus
GABA	gamma-aminobutyric acid
-ir	immunoreactive
NMDA	*N*-methyl-D-aspartate
NTS_{VL}	ventrolateral subnucleus of solitary tract nucleus
P	postnatal day
PBC	pre-Bötzinger complex
PBS	sodium phosphate buffered saline
R	receptor
SIDS	Sudden Infant Death Syndrome

REFERENCES

Barria A, Malinow R. NMDA receptor subunit composition controls synaptic plasticity by regulating binding to CaMKII. Neuron. 2005; 48:289–301. [PubMed: 16242409]

Bieger D, Hopkins DA. Viscerotopic representation of the upper alimentary tract in the medulla oblongata in the rat: the nucleus ambiguus. J Comp Neurol. 1987; 262:546. [PubMed: 3667964]

Blanco CE, Dawes GS, Hanson MA, McCooke HB. The response to hypoxia of arterial chemoreceptors in fetal sheep and new-born lambs. J Physiol. 1984; 351:25–37. [PubMed: 6747866]

Bonham AC. Neurotransmitters in the CNS control of breathing. Respir Physiol. 1995; 101:219–230. [PubMed: 8606995]

Bosman LWJ, Rosahl TW, Brussaard AB. Neonatal development of the rat visual cortex: synaptic function of $GABA_A$ receptor α subunits. J Physiol. 2002; 545:169–181. [PubMed: 12433958]

Brickley SG, Misra C, Mok MH, Mishina M, Cull-Candy SG. NR2B and NR2D subunits coassemble in cerebellar Golgi cells to form a distinct NMDA receptor subtype restricted to extrasynaptic sites. J Neurosci. 2003; 23:4958–4966. [PubMed: 12832518]

Brouillette RT, Waxman DH, National Academy of Clinical Biochemistry. Evaluation of the newborn's blood gas status. Clin Chem. 1997; 43:215–221. [PubMed: 8990256]

Cathala L, Misra C, Cull-Candy S. Developmental profile of the changing properties of NMDA receptors at cerebellar mossy fiber-granule cell synapses. J Neurosci. 2000; 20:5899–5905. [PubMed: 10934236]

Cavara NA, Orth A, Hollmann M. Effects of NR1 splicing on NR1/NR3B-type excitatory glycine receptors. BMC Neurosci. 2009; 10:32. [PubMed: 19348678]

Chatterton JE, Awobuluyi M, Premkumar LS, Takahashi H, Talantova M, Shin Y, Cui J, Tu S, Sevarino KA, Nakanishi N, Tong G, Lipton SA, Zhang D. Excitatory glycine receptors containing the NR3 family of NMDA receptor subunits. Nature. 2002; 415:793–798. [PubMed: 11823786]

Chen N, Luo T, Raymond LA. Subtype-dependence of NMDA receptor channel open probability. J Neurosci. 1999; 19(16):6844–6854. [PubMed: 10436042]

Coles SK, Ernsberger P, Dick TE. A role for NMDA receptors in posthypoxic frequency decline in the rat. Am J Physiol. 1998; 274:R1546–1555. [PubMed: 9608007]

Cull-Candy SG, Leszkiewicz DN. Role of distinct NMDA receptor subtypes at central synapses. Sci STKE. 2004; 255:re16. [PubMed: 15494561]

Czapla MA, Simakajornboon N, Holt GA, Gozal D. Tyrosine kinase inhibitors modulate the ventilatory response to hypoxia in the conscious rat. J Appl Physiol. 1999; 87:363–369. [PubMed: 10409596]

Davis SE, Solhied G, Castillo M, Dwinell M, Brozoski D, Forster HV. Postnatal developmental changes in CO2 sensitivity in rats. J Appl Physiol. 2006; 101:1097–1103. [PubMed: 16794027]

Dogaš Z, Stuth EA, Hopp FA, McCrimmon DR, Zuperku EJ. NMDA receptor-mediated transmission of carotid body chemoreceptor input to expiratory bulbospinal neurones in dogs. J Physiol. 1995; 487:639–651. [PubMed: 8544127]

Dumas TC. Developmental regulation of cognitive abilities: modified composition of a molecular switch turns on associative learning. Prog Neurobiol. 2005; 76:189–211. [PubMed: 16181726]

Durand GM, Marandi N, Herberger SD, Blum R, Konnerth A. Quantitative single-cell RT-PCR and Ca2+ imaging in brain slices. Pflugers Arch. 2006; 451:716–726. [PubMed: 16211366]

Eden GJ, Hanson MA. Maturation of the respiratory response to acute hypoxia in the newborn rat. J Physiol. 1987; 392:1–9. [PubMed: 3446776]

Ellefsen S, Sandvik GK, Larsen HK, Stensløkken KO, Hov DA, Kristensen TA, Nilsson GE. Expression of genes involved in excitatory neurotransmission in anoxic crucian carp (Carassius carassius) brain. Physiol Genomics. 2008; 35:5–17. [PubMed: 18593861]

Erreger K, Dravid SM, Banke TG, Wyllie DJ, Traynelis SF. Subunit-specific gating controls rat NR1/NR2A and NR1/NR2B NMDA channel kinetics and synaptic signalling profiles. J Physiol. 2005; 563:345–358. [PubMed: 15649985]

Feldman JL, Windhorst U, Anders K, Richter DW. Synaptic interaction between medullary respiratory neurones during apneusis induced by NMDA-receptor blockade in cat. J Physiol. 1992; 450:303–323. [PubMed: 1432710]

Finley JCW, Katz DM. The central organization of carotid body afferent projection to the brain stem of the rat. Brain Res. 1992; 572:108–116. [PubMed: 1611506]

Gray PA, Rekling JC, Bocchiaro CM, Feldman JL. Modulation of respiratory frequency by peptidergic input to rhythmogenic neurons in the pre-Bötzinger complex. Science. 1999; 286:1566–1568. [PubMed: 10567264]

Horner RL. Respiratory motor activity: influence of neuromodulators and implications for sleep disordered breathing. Can J Physiol Pharmacol. 2007; 85:155–165. [PubMed: 17487255]

Jordan D. Central nervous pathways and control of the airways. Respir Physiol. 2001; 125:67–81. [PubMed: 11240153]

Kron M, Reuter J, Gerhardt E, Manzke T, Zhang W, Dutschmann M. Emergence of brain-derived neurotrophic factor-induced postsynaptic potentiation of NMDA currents during the postnatal maturation of the Kolliker-Fuse nucleus of rat. J Physiol. 2008; 586:2331–2343. [PubMed: 18339694]

Kubota S, Kitajima T. A model for synaptic development regulated by NMDA receptor subunit expression. J Comput Neurosci. 2008; 24:1–20. [PubMed: 18202921]

Liu Q, Wong-Riley MTT. Postnatal expression of neurotransmitters, receptors, and cytochrome oxidase in the rat pre-Bötzinger complex. J Appl Physiol. 2002; 92:923–934. [PubMed: 11842022]

Liu Q, Wong-Riley MTT. Postnatal changes in cytochrome oxidase expressions in brain stem nuclei of rats: implications for sensitive periods. J Appl Physiol. 2003; 95:2285–2291. [PubMed: 12909612]

Liu Q, Wong-Riley MTT. Developmental changes in the expression of GABAA receptor subunits alpha1, alpha2, and alpha3 in the rat pre-Bötzinger complex. J Appl Physiol. 2004; 96:1825–1831. [PubMed: 14729731]

Liu Q, Wong-Riley MTT. Postnatal developmental expressions of neurotransmitters and receptors in various brain stem nuclei of rats. J Appl Physiol. 2005; 98:1442–1457. [PubMed: 15618314]

Liu Q, Wong-Riley MTT. Developmental changes in the expression of GABA(A) receptor subunits alpha1, alpha2, and alpha3 in brain stem nuclei of rats. Brain Res. 2006; 1098:129–138. [PubMed: 16750519]

Liu Q, Wong-Riley MT. Postnatal changes in the expression of serotonin 2A receptors in various brain stem nuclei of the rat. J Appl Physio. 2008; 104:1801–1808.

Liu Q, Kim J, Cinotte J, Homolka P, Wong-Riley MT. Carotid body denervation effect on cytochrome oxidase activity in pre-Bötzinger complex of developing rats. J Appl Physiol. 2003; 9:1115–1121. [PubMed: 12571139]

Liu Q, Lowry TF, Wong-Riley MT. Postnatal changes in ventilation during normoxia and acute hypoxia in the rat: implication for a sensitive period. J Physiol. 2006; 577:957–970. [PubMed: 17038423]

Liu Q, Fehring C, Lowry TF, Wong-Riley MT. Postnatal development of metabolic rate during normoxia and acute hypoxia in rats: implication for a sensitive period. J Appl Physiol. 2009; 106:1212–1222. [PubMed: 19118157]

Liu XB, Murray KD, Jones EG. Switching of NMDA receptor 2A and 2B subunits at thalamic and cortical synapses during early postnatal development. J Neurosci. 2004; 24:8885–8895. [PubMed: 15470155]

Liu YY, Wong-Riley MT. Developmental study of cytochrome oxidase activity in the brain stem respiratory nuclei of postnatal rats. J Appl Physiol. 2001; 90:685–694. [PubMed: 11160070]

Matsuda K, Kamiya Y, Matsuda S, Yuzaki M. Cloning and characterization of a novel NMDA receptor subunit NR3B: a dominant subunit that reduces calcium permeability. Brain Res Mol Brain Res. 2002; 100:43–52. [PubMed: 12008020]

McGuire M, Zhang Y, White DP, Ling L. Phrenic long-term facilitation requires NMDA receptors in the phrenic motonucleus in rats. J Physiol. 2005; 567:599–611. [PubMed: 15932891]

McGuire M, Liu C, Cao Y, Ling L. Formation and maintenance of ventilatory long-term facilitation require NMDA but not non-NMDA receptors in awake rats. J Appl Physiol. 2008; 105:942–950. [PubMed: 18583381]

Monyer H, Burnashev N, Laurie DJ, Sakmann B, Seeburg PH. Developmental and regional expression in the rat brain and functional properties of four NMDA receptors. Neuron. 1994; 12:529–540. [PubMed: 7512349]

Morgado-Valle C, Feldman JL. NMDA receptors in preBotzinger complex neurons can drive respiratory rhythm independent of AMPA receptors. J Physiol. 2007; 582:359–368. [PubMed: 17446224]

Mortola, JP. Respiratory Physiology of Newborn Mammals. The Johns Hopkins University Press; Baltimore: 2001.

Nishi M, Hinds H, Lu HP, Kawata M, Hayashi Y. Motoneuron-specific expression of NR3B, a novel NMDA-type glutamate receptor subunit that works in a dominant-negative manner. J Neurosci. 2001; 21:RC185. [PubMed: 11717388]

Ohtake PJ, Torres JE, Gozal YM, Graff GR, Gozal D. NMDA receptors mediate peripheral chemoreceptor afferent input in the conscious rat. J Appl Physiol. 1998; 84:853–861. [PubMed: 9480943]

Ohtake PJ, Simakajornboon N, Fehniger MD, Xue YD, Gozal D. N-Methyl-D-aspartate receptor expression in the nucleus tractus solitarii and maturation of hypoxic ventilatory response in the rat. Am J Respir Crit Care Med. 2000; 162:1140–1147. [PubMed: 10988143]

Okada M, Onodera K, Van Renterghem C, Sieghart W, Takahashi T. Functional correlation of GABA(A) receptor alpha subunits expression with the properties of IPSCs in the developing thalamus. J Neurosci. 2000; 20:2202–2208. [PubMed: 10704495]

Pace RW, Mackay DD, Feldman JL, Del Negro CA. Inspiratory bursts in the preBötzinger complex depend on a calcium-activated non-specific cation current linked to glutamate receptors in neonatal mice. J Physiol. 2007; 582:113–125. [PubMed: 17446214]

Paton JF, Richter DW. Maturational changes in the respiratory rhythm generator of the mouse. Pflügers Arch. 1995; 430:115–124.

Paton JF, Rogers WT, Schwaber JS. Tonically rhythmic neurons within a cardiorespiratory region of the nucleus tractus solitarii of the rat. J Neurophysiol. 1991; 66:824–838. [PubMed: 1684382]

Pierrefiche O, Foutz AS, Champagnat J, Denavit-Saubié M. NMDA and non-NMDA receptors may play distinct roles in timing mechanisms and transmission in the feline respiratory network. J Physiol. 1994; 474:509–523. [PubMed: 8014910]

Poon CS, Zhou Z, Champagnat J. NMDA receptor activity in utero averts respiratory depression and anomalous long-term depression in newborn mice. J Neurosci. 2000; 20:RC73. [PubMed: 10777815]

Prybylowski KL, Grossman SD, Wrathall JR, Wolfe BB. Expression of splice variants of the NR1 subunit of the N-methyl-D-aspartate receptor in the normal and injured rat spinal cord. J Neurochem. 2001; 76:797–805. [PubMed: 11158251]

Reeves SR, Gozal E, Guo SZ, Sachleben LR Jr, Brittian KR, Lipton AJ, Gozal D. Effect of long-term intermittent and sustained hypoxia on hypoxic ventilatory and metabolic responses in the adult rat. J Appl Physiol. 2003; 95:1767–1774. [PubMed: 14555663]

Rekling JC, Feldman JL. Pre-Bötzinger complex and pacemaker neurons: hypothesized site and kernel for respiratory rhythm generation. Annu Rev Physiol. 1998; 60:385–405. [PubMed: 9558470]

Sheng M, Cummings J, Roldan LA, Jan YN, Jan LY. Changing subunit composition of heteromeric NMDA receptors during development of rat cortex. Nature. 1994; 368:144–147. [PubMed: 8139656]

Smith JC, Ellenberger HH, Ballanyi K, Richter DW, Feldman JL. Pre-Bötzinger complex: a brain stem region that may generate respiratory rhythm in mammals. Science. 1991; 254:726–729. [PubMed: 1683005]

Smith JC, Butera RJ, Koshiya N, Negro CD, Wilson CG, Johnson SM. Respiratory rhythm generation in neonatal and adult mammals: the hybrid pacemaker-network model. Respir Physiol. 2000; 122:131–147. [PubMed: 10967340]

Takahashi T, Feldmeyer D, Suzuki N, Onodera K, Cull-Candy SG, Sakimura K, Mishina M. Functional correlation of NMDA receptor epsilon subunits expression with the properties of single-channel and synaptic currents in the developing cerebellum. J Neurosci. 1996; 16:4376–4382. [PubMed: 8699248]

Tarakanov I, Dymecka A, Pokorski M. NMDA glutamate receptor antagonism and the ventilatory response to hypoxia in the anesthetized rat. J Physiol Pharmacol. 2004; 55(S3):139–147. [PubMed: 15611606]

von Engelhardt J, Doganci B, Jensen V, Hvalby Ø , Göngrich C, Taylor A, Barkus C, Sanderson DJ, Rawlins JN, Seeburg PH, Bannerman DM, Monyer H. Contribution of hippocampal and extra-hippocampal NR2B-containing NMDA receptors to performance on spatial learning tasks. Neuron. 2008; 60:846–860. [PubMed: 19081379]

Watanabe M, Inoue Y, Sakimura K, Mishina M. Developmental changes in distribution of NMDA receptor channel subunit mRNAs. Neuroreport. 1992; 3:1138–1140. [PubMed: 1493227]

Waters KA, Machaalani R. Role of NMDA receptors in development of respiratory control. Respir Physiol Neurobiol. 2005; 149:123–130. [PubMed: 15908286]

Wong-Riley MTT, Liu Q. Neurochemical development of brain stem nuclei involved in the control of respiration. Respir Physiol Neurobiol. 2005; 149:83–98. [PubMed: 16203213]

Wong-Riley MT, Liu Q. Neurochemical and physiological correlates of a critical period of respiratory development in the rat. Respir Physiol Neurobiol. 2008; 164:28–37. [PubMed: 18524695]

Yashiro K, Philpot BD. Regulation of NMDA receptor subunit expression and its implications for LTD, LTP, and metaplasticity. Neuropharmacol. 2008; 55:1081–1094.

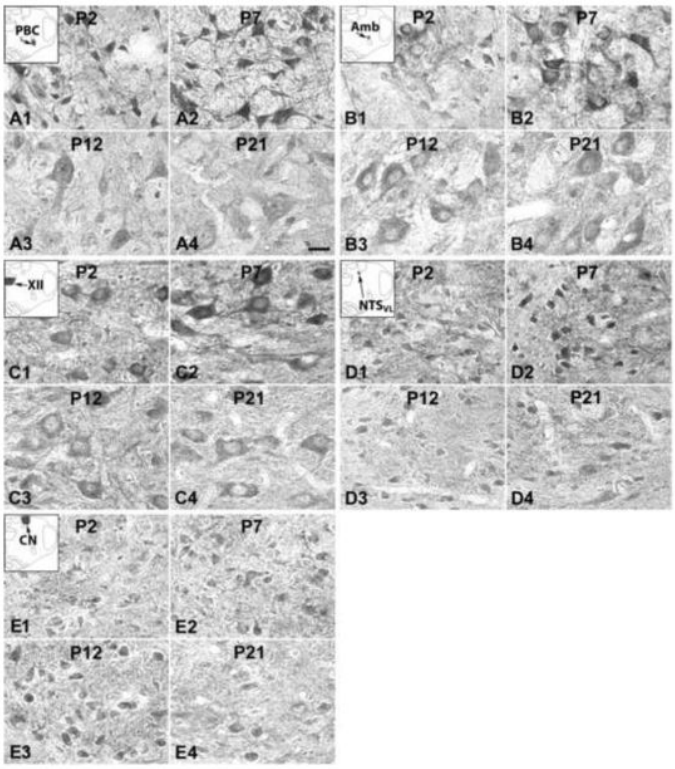

Fig. 1.

N-methyl-D-aspartate receptors (NR) subunits 2A (NR2A) immunoreactive (-ir) neurons in the pre-Bötzinger complex (PBC) (A), nucleus ambiguus (Amb) (B), hypoglossal nucleus (XII) (C), ventrolateral subnucleus of the solitary tract nucleus (NTS_{VL}) (D), and cuneate nucleus (CN) (E) at representative postnatal days P2 (A1-E1), P7 (A2-E2), P12 (A3-E3), and P21 (A4-E4). The insets in A1-E1 indicate the locations of each nucleus in a diagrammatic cross section of the medulla. The expression of NR2A-ir in the PBC, Amb, XII, and NTS_{VL} neurons increased at P7 (compared with that at P2), but was significantly decreased at P12, followed by a plateau or a decline at P21. The NR2A-ir expression in the CN neurons was relatively constant at four ages presented. Scale bar: 20 μm for all.

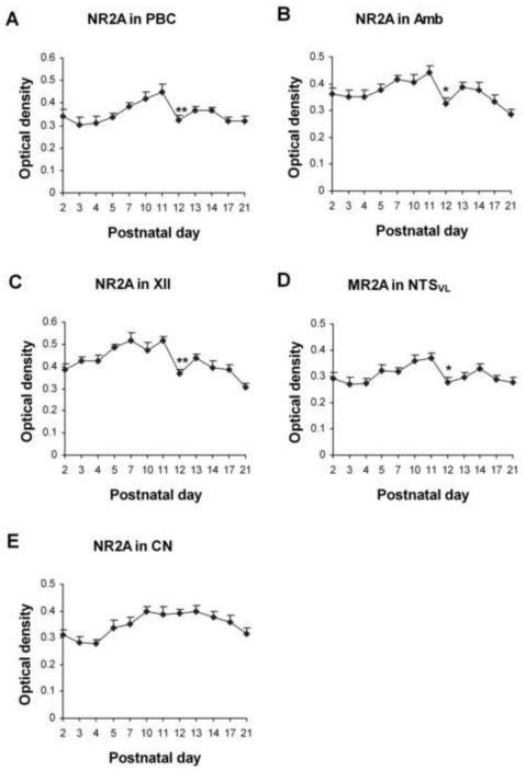

Fig. 2.

Optical densitometric measurements of immunoreactive product for NR2A in the cytoplasm of individual neurons in the PBC (A), Amb (B), XII (C), NTS_{VL} (D), and CN (E) from P2 to P21. Data points were presented as mean ± SEM. The NR2A-ir expression in the first four nuclei exhibited a gradual increase from P2 or P3 to P11, then a distinct fall at P12, followed by a small rise and a plateau or a gradual decline until P21. The expression in the CN was relatively constant from P2 to P21. ANOVA yielded significant differences in the NR2A expression among ages in all four respiratory nuclei examined ($P < 0.01$). Tukey's Studentized test revealed a significant reduction at P12 as compared to P11 ($P < 0.01$ for the PBC and XII, $P < 0.05$ for the Amb and NTS_{VL}). These graphs in Fig. 2 (as well as those in Figs. 4, 6, 8, and 10) show significance only between one age group and its immediately adjacent younger age groups as analyzed by Tukey's test. Additional significant differences between any two age groups can be found in the text. *, $P < 0.05$; **, $P < 0.01$ (Tukey's Studentized test).

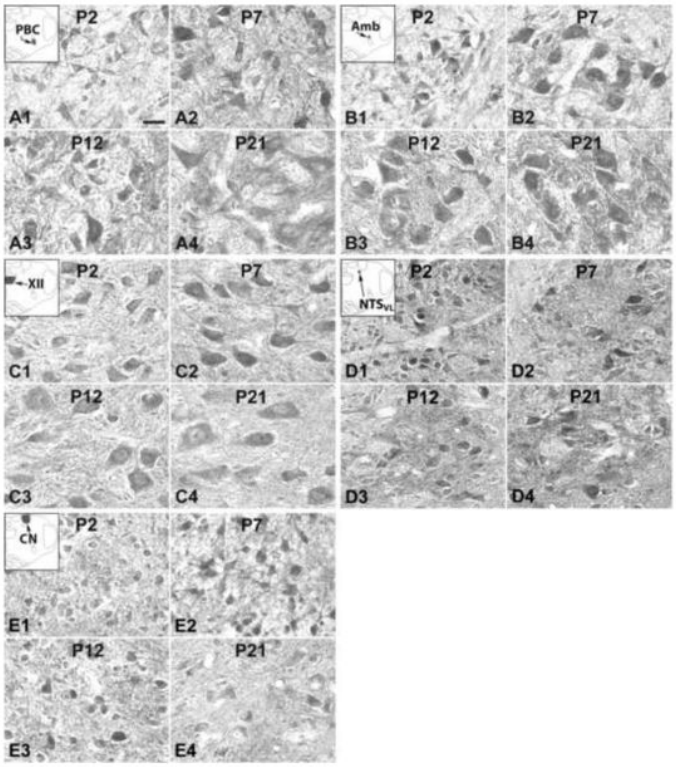

Fig. 3.

NR2B-ir neurons in the PBC (A), Amb (B), XII (C), NTS_{VL} (D), and CN (E) at P2 (A1-E1), P7 (A2-E2), P12 (A3-E3), and P21 (A4-E4). The insets in A1-E1 indicate the locations of each nucleus in a diagrammatic cross section of the medulla. The NR2B-ir expression in all five nuclei was relatively constant at the four ages shown. Scale bar: 20 μm for all.

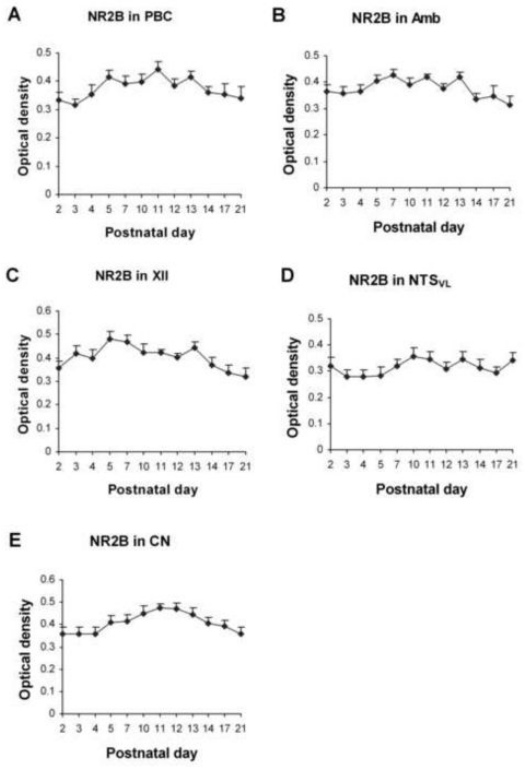

Fig. 4.

Optical densitometric measurements of immunoreactive product for NR2B in the cytoplasm of individual neurons in the PBC (A), Amb (B), XII (C), NTS_{VL} (D), and CN (E) from P2 to P21. Data points were presented as mean ± SEM. The expression of NR2B-ir in neurons of all five nuclei was relatively stable during the first three postnatal weeks, with only minor fluctuations throughout. ANOVA failed to reveal any significant differences among the ages in all five nuclei examined ($P > 0.01$).

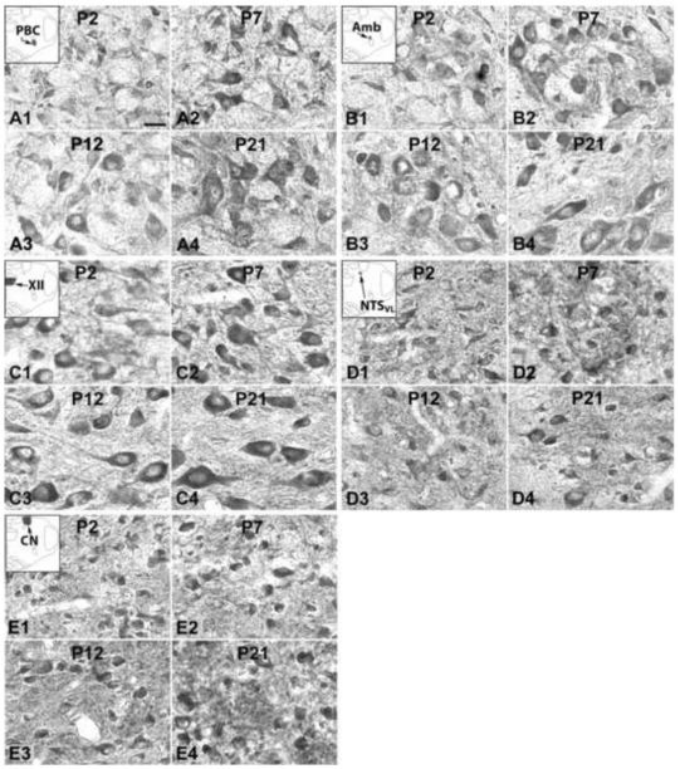

Fig. 5.

NR2C-ir neurons in the PBC (A), Amb (B), XII (C), NTS_{VL} (D), and CN (E) at P2 (A1-E1), P7 (A2-E2), P12 (A3-E3), and P21 (A4-E4). The insets in A1-E1 indicate the locations of each nucleus in a diagrammatic cross section of the medulla. In all five nuclei, NR2C-ir expression showed the lowest level at P2, a rise at P7, followed by a plateau at P12 and P21, with a noted exception in the PBC, which had a significant reduction at P12. Scale bar: 20 μm for all.

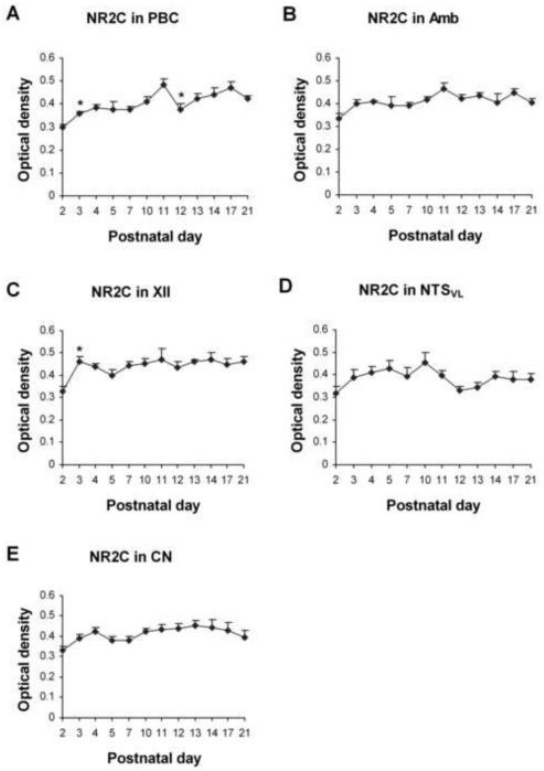

Fig. 6.

Optical densitometric measurements of immunoreactive product for NR2C in the cytoplasm of individual neurons in the PBC (A), Amb (B), XII (C), NTS_{VL} (D), and CN (E) from P2 to P21. Data points were presented as mean ± SEM. The NR2C-ir expression was the lowest at P2, increased with or without statistical significance at P3, followed by a plateau until P21. A distinct exception was found in the PBC, which showed a significant reduction at P12 ($P < 0.05$). ANOVA revealed significant differences ($P < 0.01$) in the NR2C-ir expression among the ages in the PBC and XII, and Tukey's test indicated a significant rise at P3 for the PBC and XII ($P < 0.05$), and significant reduction at P12 for the PBC ($P < 0.05$). *, $P < 0.05$ (Tukey's Studentized test).

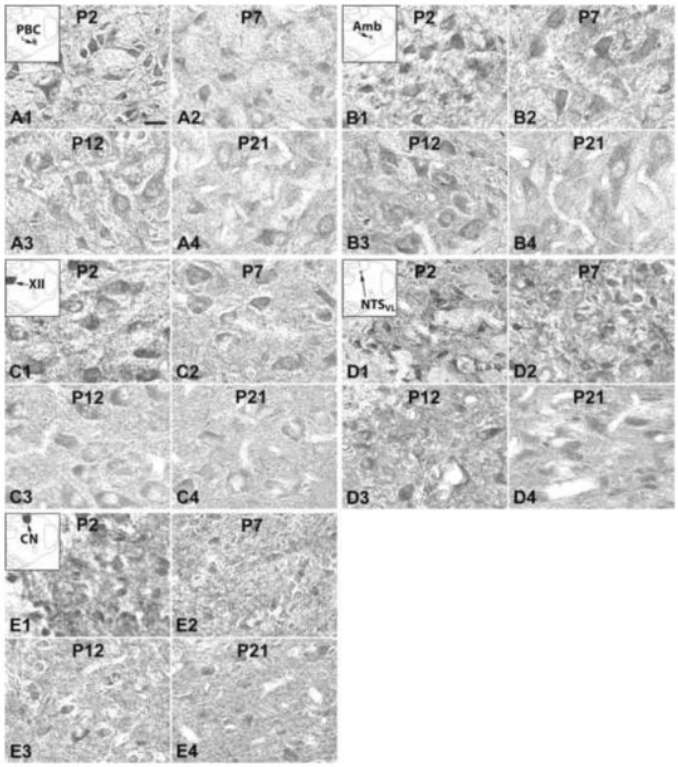

Fig. 7.

NR2D-ir neurons in the PBC (A), Amb (B), XII (C), NTS_{VL} (D), and CN (E) at P2 (A1-E1), P7 (A2-E2), P12 (A3-E3), and P21 (A4-E4). The insets in A1-E1 indicate the locations of each nucleus in a diagrammatic cross section of the medulla. In all five nuclei, NR2D-ir expression demonstrated the highest level at P2, declining at P7, followed by a plateau at P12, and decreased again at P21, except for NTS_{VL} in which the expression at P21 was comparable to that at P12. Scale bar: 20 μm for all.

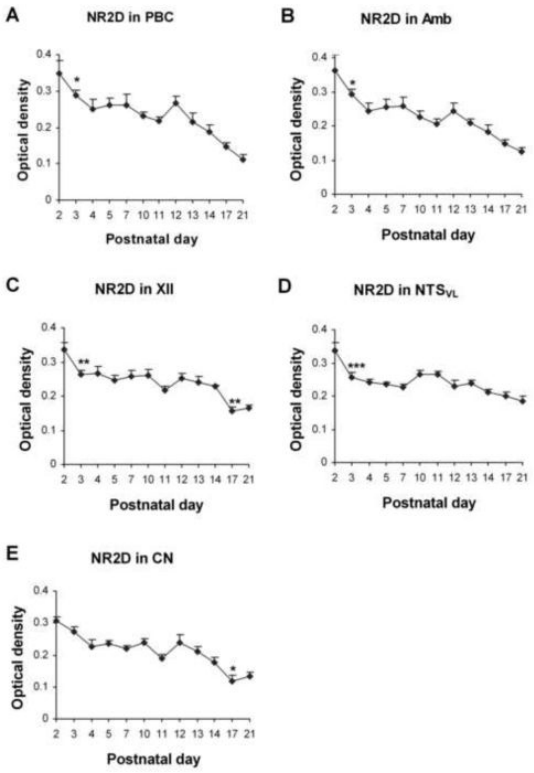

Fig. 8.

Optical densitometric measurements of immunoreactive product for NR2D in the cytoplasm of individual neurons in the PBC (A), Amb (B), XII (C), NTS_{VL} (D), and CN (E) from P2 to P21. Data points were presented as mean ± SEM. NR2D-ir exhibited the highest levels at P2, significantly reduced at P3 for the four respiratory related nuclei, followed by a plateau until P12, then declined again until P17-21. ANOVA revealed significant differences ($P < 0.01$) among the ages in all five nuclei, and Tukey's test indicated a significant reduction in the expression at P3 for the four nuclei ($P < 0.05$ for the PBC and Amb, $P < 0.01$ for the XII, and $P < 0.001$ for the NTS_{VL}), and another significant reduction at P17 for the XII ($P < 0.01$) and CN ($P < 0.05$). *, $P < 0.05$; **, $P < 0.01$; ***, $P < 0.001$ (Tukey's test).

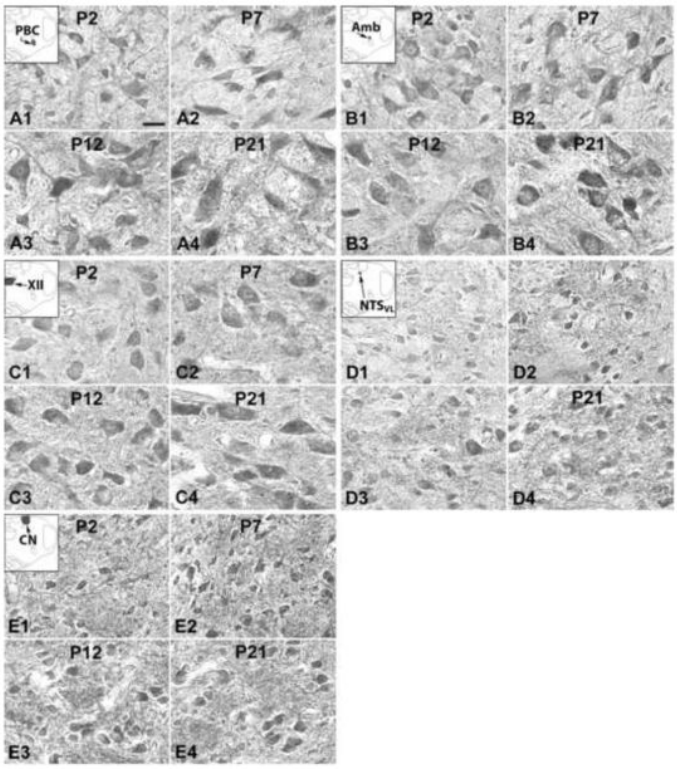

Fig. 9.

NR3B-ir neurons in the PBC (A), Amb (B), XII (C), NTS_{VL} (D), and CN (E) at P2 (A1-E1), P7 (A2-E2), P12 (A3-E3), and P21 (A4-E4). The insets in A1-E1 indicate the locations of each nucleus in a diagrammatic cross section of the medulla. In the PBC, Amb, XII, and NTS_{VL}, the expression of NR3B-ir was lowest at P2, increased at P7, followed by a further rise (PBC and Amb) or a plateau (XII and NTS_{VL}) at P12 and P21. In the CN, however, the expression remained relatively constant during development. Scale bar: 20 μm for all.

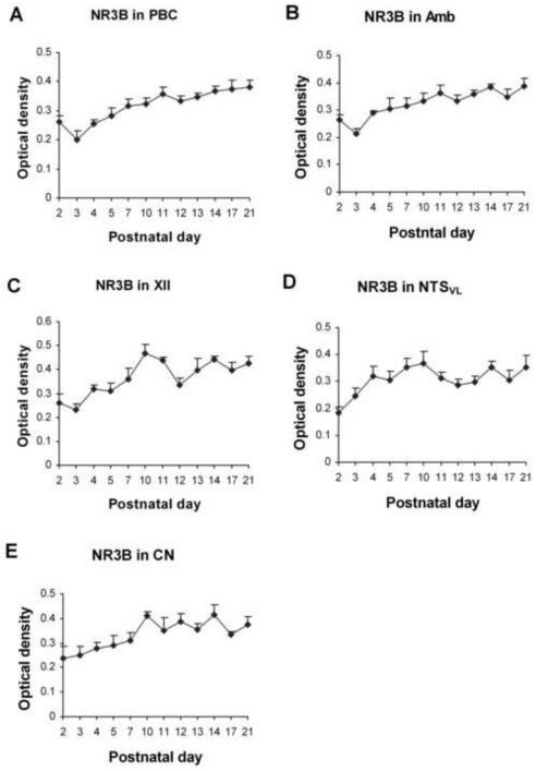

Fig. 10.

Optical densitometric measurements of immunoreactive product for NR3B in the cytoplasm of individual neurons in the PBC (A), Amb (B), XII (C), NTS_{VL} (D), and CN (E) from P2 to P21. Data points were presented as mean ± SEM. In the PBC, Amb, and XII, the NR3B-ir exhibited a statistically insignificant dip at P3, followed by a gradual increase until P21, whereas in the NTS_{VL}, the rise from P2 to P4, or from P2 to P10, was gradual and it was followed by a plateau until P21. The XII and NTS_{VL} had another statistically insignificant reduction at P11-12. In the CN, NR3B-ir was relatively constant from P2 to P21, with a gentle rise mainly between P2 and P10, after which it plateaued until P21. ANOVA yielded significant differences ($P < 0.01$) among the ages in the PBC, Amb and XII, but Tukey's Studentized range test that compared one age group with its adjacent younger age group failed to reveal statistical significance in any comparison between paired adjacent age groups ($P > 0.05$).

Table 1

Primary antibodies used

Antigen	Immunogen	Manufacturer, species, type, catalog number	Dilution used
NE2A	C-terminal fusion protein of rat NR2A, aa 1253-1391	Chemicon (Temecula, CA), rabbit polyclonal, #AB1555P	1:500
NR2B	C-terminal fusion protein of NR2B (30 kDa)	Chemicon (Temecula, CA), rabbit polyclonal, #AB1557P	1:1000
NR2C	Amino acid 21-100 mapping near the N-terminus of human NR2C	Santa Cruz Biotech (Santa Cruz, CA), rabbit polyclonal, #sc-50437	1:600
NR2D	Recombinant protein from rat NR2D	Chemicon (Temecula, CA), mouse monoclonal, #MAB5578	1:300
NR3B	Amino acid 916-930 of mouse NR3B	Upstate (Temecula, CA), rabbit polyclonal, #07-351	1:200